

# Architecture Trade Study for the Terrestrial Planet Finder Interferometer

Oliver P. Lay<sup>\*</sup>, Steven M. Gunter, Louise A. Hamlin, Curt A. Henry, Ying-Yong Li,  
Stefan R. Martin, George H. Purcell Jr., Brent Ware  
Jet Propulsion Laboratory, California Institute of Technology, 4800 Oak Grove Drive,  
Pasadena, CA 91109

Julie A. Wertz  
Space Systems Laboratory, Massachusetts Institute of Technology, Cambridge, MA

M. Charley Noecker  
Ball Aerospace & Technologies Corp., 1600 Commerce St., Boulder, CO, 80301

## ABSTRACT

The Terrestrial Planet Finder Interferometer (TPF-I) is a space-based NASA mission for the direct detection of Earth-like planets orbiting nearby stars. At the mid-infrared wavelength range of interest, a sun-like star is  $\sim 10^7$  times brighter than an earth-like planet, with an angular offset of  $\sim 50$  mas. A set of formation-flying collector telescopes direct the incoming light to a common location where the beams are combined and detected. The relative locations of the collecting apertures, the way that the beams are routed to the combiner, and the relative amplitudes and phases with which they are combined constitute the architecture of the system. This paper evaluates six of the most promising solutions: the Linear Dual Chopped Bracewell (DCB), X-Array, Diamond DCB, Z-Array, Linear-3 and Triangle architectures.

Each architecture is constrained to fit inside the shroud of a Delta IV Heavy launch vehicle using a parametric model for mass and volume. Both single and dual launch options are considered. The maximum separation between spacecraft is limited by stray light considerations. Given these constraints, the performance of each architecture is assessed by modeling the number of stars that can be surveyed and characterized spectroscopically during the mission lifetime, and by modeling the imaging properties of the configuration and the robustness to failures. The cost and risk for each architecture depends on a number of factors, including the number of launches, and mass margin. Quantitative metrics are used where possible.

A matrix of the architectures and  $\sim 30$  weighted discriminators was formed. Each architecture was assigned a score for each discriminator. Then the scores were multiplied by the weights and summed to give a total score for each architecture. The X-Array and Linear DCB were judged to be the strongest candidates. The simplicity of the three-collector architectures was not rated to be sufficient to compensate for their reduced performance and increased risk. The decision process is subjective, but transparent and easily adapted to accommodate new architectures and differing priorities.

Keywords: Optical interferometry, nulling, planet detection

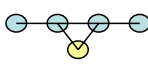
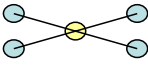
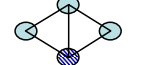
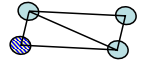
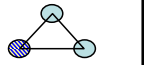
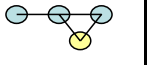
## 1. INTRODUCTION

There is currently a large effort to find and study Earth-like planets around other stars. A number of indirect detection schemes for the detection of planets are either in use or planned in the near future. These include radial velocity measurements, astrometric wobble, and transit photometry.<sup>1,2</sup> None of these approaches detects light originating from the planet itself. The challenge for such a direct detection is the combination of large contrast ratio between the star and planet ( $\sim 10^7$  in the mid-IR;  $\sim 10^{10}$  in the visible) and the small angular separation (a maximum of 0.1 arcsec or 0.5  $\mu$ rad

---

<sup>\*</sup> [oliver.p.lay@jpl.nasa.gov](mailto:oliver.p.lay@jpl.nasa.gov); phone 1 818 354-2521; fax 1 818 393-4950

Table 1: Single-launch architecture options considered in trade study

Name	Linear DCB	X-Array (2:1)	Diamond DCB	Z-Array	Triangle	Linear 3
Configuration						
# launches	1	1	1	1	1	1
Aperture	3.8 m	3.8 m	4.1 m	4.1 m	4.1 m	4.1 m
Min size	60 m	66 m	35 m	66 m	20 m	40 m
Max size	240 m	160 m	139 m	89 m	80 m	160 m

for the Earth-Sun at a distance of 10 pc). The technique of nulling interferometry<sup>3,4</sup> has been proposed to meet this challenge, and is being pursued by both the National Aeronautics and Space Agency (the Terrestrial Planet Finder Interferometer mission<sup>5</sup>, TPF-I) and the European Space Agency (the Darwin mission<sup>6</sup>).

Over the last few years a large number of interferometric nulling configurations have been proposed, including both structurally-connected and formation-flying configurations. Initial studies of structurally-connected options for TPF showed that they were unlikely to meet the full mission requirements, and subsequent work has focused on formation flying missions. The goal of the trade study described in this paper was to pick the most promising architecture for more detailed study by the TPF-I flight design team. It is by no means a final selection for the mission, and we will continue to actively seek new designs. It is intended that the trade study analysis presented here will provide a framework that is easily expanded to include both new configurations and new analysis as they become available.

The next section describes the 6 architectures that were selected for the trade study, and the constraints that were imposed on them. Section 3 describes the scoring process, and Section 4 covers the mandatory pass/fail criteria for the designs. The large number of discriminators (“Wants”) are summarized in Section 5 (Performance) and Section 6 (Cost and risk), followed by a discussion of the results and suggestions for future studies (Section 7) and a Summary in Section 8. A complete description of the analysis that underpins the trade study is beyond the scope of this paper; the results are summarized in a series of tables, and the text is used to provide additional information for a limited subset of the issues.

## 2. ARCHITECTURES & CONSTRAINTS

We define an architecture by the combination of nulling configuration, collector aperture diameter, beam routing between spacecraft, beam combiner design, number of launches and type of launch vehicle. The nulling configuration includes the number and relative locations of the collectors, and the amplitudes and phases with which each collector beam is combined. All are significantly constrained in geometry by the need for equal optical path lengths from each collector to the combiner

The 6 basic architectures compared in this study are listed in Table 1, ranging from 3 to 5 spacecraft. The first four are all part of the Dual Chopped Bracewell (DCB) family, in which the 4 apertures have phases of  $0$ ,  $\pi/2$ ,  $\pi$  and  $3\pi/2$  radians. The Linear DCB<sup>7</sup> can be phased in two ways, with either separated or interleaved nulling baselines. In the analysis we choose the optimal case for each observing scenario. The X-Array<sup>8</sup> chosen for study has a fixed 2:1 aspect ratio (a tunable aspect ratio is discussed in Section 7). The Diamond DCB and Z-Array were both proposed by Anders Karlsson (private communication) as a means of reducing the number of spacecraft; the hatched circle in the schematic indicates a spacecraft that functions as both a collector and combiner. The Z-Array uses multiple relays between the collectors to balance the path lengths. The 4 DCB architectures have identical beam combiners. The Triangle and Linear 3 are based on a 3-way nulling strategy<sup>9</sup> with phases of  $0$ ,  $2\pi/3$  and  $4\pi/3$ . In all cases, the spacecraft are confined to a plane perpendicular to the target star direction for thermal reasons. The beams must be routed such that the path lengths from the star to the combiner are equal; this is achieved with a single hop from the collector to the combiner in the X-Array, two hops for the Linear DCB, Diamond DCB, Triangle and Linear 3, and up to 4 hops for the Z-Array. Many nulling configurations were not considered here: the single Bracewell nuller is too sensitive to systematic effects (see Section 4), and the so-called  $\theta^4$  class of configurations with broader nulls have previously been shown to be significantly less efficient at detecting planets<sup>10</sup>. The 6 chosen architectures represent basic, no-frills designs for planet-finding, without upgrades for added redundancy or enhanced astrophysics capability. Additional constraints, as described below, were applied to determine the aperture diameter, and the limits to the array size listed in Table 1.

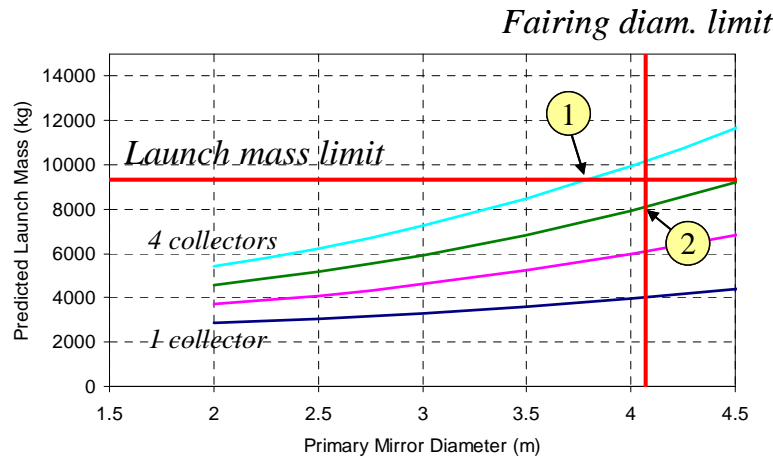


Figure 1: Launch mass as a function of primary mirror diameter and number of collectors for the case where there is a separate combiner spacecraft. Mass and fairing diameter constraints are shown for a Delta IV-Heavy launcher, assuming 30% mass margin. The maximum aperture diameter is 3.8 m for the Linear DCB and X-Array configurations, constrained by the launch mass (Point 1). The Linear 3 configuration has a maximum diameter of 4.1 m, constrained by the fairing diameter (Point 2). A modified set of curves was used for the combiner-less configurations.

and  $D^{2.0}$  for the solar shade. The mass of the combiner spacecraft and optics, and the collector spacecraft bus were assumed to be independent of the aperture size. The curves predicted by the model in the case where there is a separate combiner spacecraft are shown in Fig. 1. Also shown is the 9600 kg launch mass limit. The values in Table 1 show that the aperture is mass-limited for the Linear DCB and X-Array, but is constrained by the fairing diameter for the other architectures. The fairing height of 17 m was not the limiting constraint for any of the architectures considered, although the current 5-spacecraft single launch stack design still has some risk. A 2-launch scenario was also considered for the Linear DCB and X-Array; the aperture diameter is increased to 4.1 m, but there is the additional cost and complication of supporting two launches and a rendezvous in deep space, as discussed in Section 7.

The array size is defined by the longest baseline between any two collectors (center-to-center). The minimum sizes listed in Table 1 are determined by the closest separation we are willing to tolerate between spacecraft without significant risk of collision. A minimum spacecraft separation of 20 m was chosen, corresponding to a ‘tip-to-tip’ spacing of 5 m between sunshades that are 15 m across. The maximum array size for nulling is limited by stray light: the thermal emission from the solar shades of one spacecraft is scattered into the science beam on another spacecraft by contamination on the optics<sup>11</sup>. This scattered light easily overwhelms the other sources of noise unless the optics are baffled to completely block the thermal emission. As the separation between spacecraft is increased, the angular offset between the solar shade and the exit point of the science beam is reduced and the shade becomes harder to block. A maximum spacecraft separation of 80 m was imposed, based on the practical dimensions of the light baffle.

### 3. SCORING PROCESS

The scoring process is based on the Kepner-Tregoe<sup>12</sup> methodology. The idea is simple. The options are judged against a set of mandatory criteria (‘musts’) and a set of discriminators (‘wants’). Each ‘must’ is scored as a pass/fail for each option, whereas the ‘wants’ are weighted by importance and scored for each option on a scale of 1 to 10. Failing a mandatory criterion disqualifies the option from consideration. The highest weighted sum of the discriminator scores determines the best option.

The options in this case are the 6 architectures described in the previous section. The mandatory criteria are described in the next section. The list of discriminators (Sections 5 and 6) was established through a lengthy process of iteration, based on initial inputs from a joint TPF-Darwin workshop and then edited in a series of meetings of the TPF-I Architecture and Design Teams. This process involved representatives from Ball Aerospace, Lockheed Martin and

The aperture diameter is constrained by the launch vehicle and the number of spacecraft needed. We adopted the Boeing Delta IV-Heavy as the standard launch vehicle. We further assumed that the collector primary mirrors were circular and monolithic (i.e. no deployable segments). The dynamic envelope of the fairing has a diameter of 4.6 m. Allowing a total of 50 cm for other structure, the maximum launchable aperture diameter is 4.1 m, represented by the vertical line in Fig. 1. A parametric model was constructed to predict the total mass as a function of aperture diameter, number of collectors and whether or not a dedicated combiner spacecraft was needed. The model was based on the mass budget from a detailed design study for a 4-m diameter collector, using scaling laws of  $D^{2.5}$  for the collector primary,  $D^{1.5}$  for the secondary and support structure,

Northrop Grumman. Inputs were also solicited from the TPF Science Working Group. Participants were asked to weight the discriminators; an average of the responses was taken to determine the initial values, normalized so that the sum of all weights equals 100. The weights represent the relative importance given to the discriminators and stand alone from any consideration of the options.

Wherever possible, a discriminator was quantified using 1 or more metrics. For example, for the discriminator ‘Control system complexity’ the metric chosen was the number of control loops needed for the basic array operation. These metrics help to inform the scoring process, although scoring is fundamentally subjective. The scoring of the discriminators for each option was conducted at a 2 day meeting held at JPL in December 2004, with approximately 20 participants from JPL and the contractors. For each discriminator the best option was scored a 10, and a simple voting system was used to establish the scores for the other options. Sometimes the scores bore a linear relationship to the metrics; sometimes explicitly not. If there was little difference between the options then the scores were close together; large differences were reflected in a low score for the worst option. The contribution to the final score is given by the product of the weight and the score, with the weight reflecting the importance of the discriminator and the score showing the size of the difference between the options. The weighted sum of the scores has a maximum possible value of 1000 points for each option.

After the initial round of scoring there were multiple rounds of iteration in which both the weights and scores could be adjusted. This may sound like ‘gaming the system’, but the intent is not that we turn the crank on the process and blindly accept the outcome; rather it is that the final table should reflect the collective engineering judgment of the group. The process is inevitably subjective (particularly the assigning of weights), but is highly transparent. It structures the analysis, focuses discussion on the key areas, and invites criticism and comment.

#### 4. MANDATORY CRITERIA

The eight mandatory criteria (‘musts’) are listed in Table 2. There are two columns associated with each architecture option: the shaded column contains ‘y’ (yes/pass) or ‘n’ (no/fail) while the adjacent column to the right gives the performance metric if there is one. The first two – the number of stars that can be surveyed for planets and the number that can be characterized by spectroscopy – were assessed using the star count metric, as follows.

The star count tool uses a model of the instrument performance to predict the number of stars in the input catalog that can be observed. The model represents a key component of the performance analysis (it is also used for several of the performance discriminators) and has been described in detail elsewhere<sup>10</sup>. For planet detection we assume:

- 2 years mission time
- 3 visits per star
- 50% observing efficiency
- detection requires broadband SNR > 5 on an Earth sized planet

For spectroscopic characterization we assume:

- 3 years mission time
- 75% observing efficiency
- $\eta_{\text{earth}} = 0.1$  (i.e. 10% of stars have at least one terrestrial planet in the habitable zone).
- maximum of 9 months on a single planet
- SNR > 10 for a spectral channel 9.5 – 10  $\mu\text{m}$

In both cases we also assume that observations must be made within 45 degrees of the anti-sun direction, excluding any targets within 45 degrees of the ecliptic poles.

Both the Triangle and the Linear 3 architectures failed the mandatory spectroscopy criterion in Table 2, with 2.5 and 3.7 characterized planets, respectively. For spectroscopy it is very important that the contributions from multiple planets can be separated, so that there is no cross-contamination of the spectra and confusion in the result. For this reason, the note in the table specifies that the characterization must be performed with a high angular resolution condition for imaging, as distinct from the low angular resolution condition for detection. This high resolution condition requires that the angular resolution at  $\lambda = 10 \mu\text{m}$  is at least twice the angular offset of the planet from the star. This demands larger array sizes than for detection mode, and the poor performance of the Triangle and Linear 3 can be traced to the high stellar leakage characteristic of these arrays for a given angular resolution<sup>13</sup>. Given this failure, these architectures will be unacceptable unless the spectroscopy criterion is relaxed, or the star count analysis is found to be incorrect. Nevertheless, we carried these options forward to see how they would fare in the discriminators.

Table 2: Mandatory criteria to be satisfied by architecture options

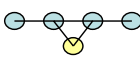
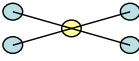
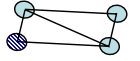
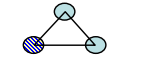
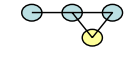
	Metric	Notes	Linear DCB		X-Array (2:1)		Diamond DCB		Z-Array		Triangle		Linear 3	
														
Number of stars surveyed (detection) > 100	Star count	With low angular resolution condition for detection	y	229	y	157	y	185	y	109	y	115	y	170
Number of stars characterized (spectroscopy) > 5 (100 x 10% x 50%)	Star count	With high angular resolution condition for imaging	y	14.2	y	13.9	y	8.8	y	9.1	n	2.5	n	3.7
Symmetric Exo-zodi suppression		Requires center-asymmetric response on the sky	y		y		y		y		y		y	
Instrument background suppression		Requires chopping scheme to remove detector gain, thermal, stray light variation	y		y		y		y		y		y	
Detect Jupiters at 5 au around 50% the stars		SWG requirement. Single-mode field of-view reqt; does not have to apply to nearest stars	y		y		y		y		y		y	
Mass margin > 30%			y	30%	y	30%	y	33%	y	33%	y	46%	y	37%
Feasible beamcombiner		Do we have a full solution?	y		y		y		y		y		y	
Feasible control system		Sufficient number of sensors and actuators?	y		y		y		y		y		y	

Table 3: Performance discriminators – number of observable targets

	Metric	Notes			Linear DCB		X-Array (2:1)		Diamond DCB		Z-Array		Triangle		Linear 3	
			Weight	Sub-weight												
<b>Performance</b>																
Number of stars surveyed (beyond minimum required)	Star count	Broadband detection, no spectroscopy	4.9	1	9.4	229	7.5	157	8.9	185	0.7	109	0.8	115	8.3	170
Number of stars located < 5 pc that can be surveyed		Nearby stars have added importance. Only 5 stars. Mid-HZ < 170 mas, so no field-of-view concern.	3.4	1	10.0	All	10.0	All	10.0	All	10.0	All	10.0	All	10.0	All
Number of stars on the coronagraph's list that can be surveyed	Star count	Ecliptic latitude limit. 28 stars common.	5.6	1	10.0	All	10.0	All	10.0	All	10.0	All	10.0	All	10.0	All
Number of planet systems characterized by spectroscopy at high angular resolution, beyond minimum required	Star count	Spatial resolution of approximately 0.5 AU (Full-Width-to-Half-Max)	5.4	1	4.2	14.2	4.5	13.9	2.0	8.8	2.2	9.1	0.0	2.5	0.0	3.7
Number of planet systems characterized by spectroscopy at low angular resolution, beyond minimum required	Star count	Spectroscopy measures a blend of any objects within and inside the habitable zone, including contribution from stellar asymmetry	2.2	1	8.3	22.5	4.8	15.1	6.3	18.2	2.0	9.1	2.7	10.4	5.2	16.2

## 5. PERFORMANCE DISCRIMINATORS

The discriminators ('wants') are divided into two categories. The performance discriminators are summarized in Tables 3, 4, and 5, while the cost and risk discriminators are addressed in Section 6. The weights given to performance sum to 43% of the maximum weighted score, compared to 57% for cost and risk.

Table 3 lists the 5 performance discriminators related to the number of stars surveyed and characterized. Again, the scores out of 10 for each option are in the shaded column, and the supporting metric is shown in the column to the right. The star count model described in the previous section was used to derive the metrics. For the three discriminators that do not show an option with the maximum score of 10, the best performance was obtained from one of the two dual-launch architectures, not included in the table. The subjectivity of the scoring is clearly evident. For example, in the case of the number of stars surveyed, one must decide how much more the 101<sup>st</sup> to 110<sup>th</sup> stars are worth, compared to the 201<sup>st</sup> to 210<sup>th</sup> stars. The low score for the Z-Array reflects the fact that it surveys only 9 stars more than the bare minimum of 100 from the mandatory criteria. The spectroscopy performance was calculated for both high (able to separate multiple planets) and low (poor separation) resolution conditions, but much more weight was given to the former. Discriminators for which the scores were identical (e.g. the number of stars surveyed closer than 5 pc) were retained in the table, since the results are nevertheless informative and future changes in the analysis or the addition of new options may break the degeneracy. In the final weighted score out of 1000, the Linear DCB will have  $4.9 \times 9.4 = 46.1$  points for number of stars surveyed, compared to  $4.9 \times 7.5 = 36.8$  points for the X-Array, and so on.

Table 4 lists the remaining 5 performance discriminators, three of which use multiple metrics. In these cases the subweight column is used to determine the extent to which each metric contributes to the overall score for that discriminator.

The fidelity of image reconstruction represents 5.7% of the overall score, and was assessed using 3 metrics. The synthesized Point Spread Function (PSF) is the analog of the 'dirty beam' function in synthesis imaging and represents the response of the instrument to a point-like planet after all the data have been combined (it is *not* the instantaneous response on the sky). The shape and structure of this function depend on the nulling configuration and the radial offset of the planet from the star<sup>13</sup>. The properties of the PSF were adopted as a proxy for planet imaging performance: the level of sidelobes relative to the peak of the PSF determine the ease of deconvolution and the associated rate of false positive and false negatives; the full-width-to-half-maximum (FWHM) of the PSF provides a measure of the angular resolution of the array (distinct from the inner working angle) and the ability to separate two nearby planets; and the number of main peaks in the PSF (some symmetric nulling configurations, e.g. the Triangle, produce a PSF with 3-fold symmetry that makes a unique deconvolution impossible). These metrics were derived for each architecture using a combination of numerical simulation (sidelobe level, FWHM) and algebraic analysis (FWHM). As an example of how the subweights are used, the rolled-up score for the Linear DCB fidelity of image reconstruction in Table 4 is given by  $0.5 \times 10 + 0.3 \times 7.2 + 0.2 \times 10 = 9.16$ . It is only this number that is used to determine the overall weighted score.

The ability of a spacecraft formation to degrade gracefully in the presence of faults was also highly weighted (4.3%). We addressed only the simple scenario of losing an entire spacecraft, and employed two metrics. The first is an estimate of the expected number of stars that an architecture will be expected to survey over the duration of the mission, relative to the ideal case, given a specified probability of losing a spacecraft. There was assumed to be a 5% probability that a given spacecraft would fail prior to observing operations, and an additional 5% probability of failure before the end of the mission, uniformly distributed in time. These failure rates were doubled to 10% for spacecraft that served as both collector and combiner. For each spacecraft in the array it was necessary to compute, using the star count model, the performance of the degraded state in which that spacecraft was absent. A simple statistical model was then applied to aggregate the performance over the length of the mission. It was assumed that the relative locations of the remaining spacecraft could not be changed, but that the array could be re-phased. There was little spread in the scores; arrays with few spacecraft had a lower chance of failure but no viable degraded states, while the Linear DCB and X-Array had higher failure rates but useful degraded states. The second metric again gives the fraction of the original number of stars that can be observed, but this time assuming that a spacecraft has been lost at the start. It rewards those architectures that degrade gracefully.



Initial estimates indicate that calibration of the relative amplitudes and phases of the array may take up to 25% of the mission time, and that the time needed will increase with the number of collectors. Star spots are a potential problem, since they have the same signature in the array output as a close-in planet. Our analysis shows that the extent of this confusion depends on the ratio of the array angular resolution (i.e. the FWHM of the PSF) to the angle subtended by the planet and the star. The discriminator for general astrophysics potential was based on four metrics which are self-explanatory in the table. Again, the values for the metrics for each architecture are shown in the unshaded columns to the right of the corresponding score.

## 6. COST AND RISK DISCRIMINATORS

Cost and risk issues represent 57% of the overall weighted score. The architectures have not been costed explicitly. Instead, a number of factors, mostly related to the expected design complexity, are used as proxies for the cost. These are listed in Tables 5 and 6. In many cases, we leave the text and values in the tables to speak for themselves. The text below provides additional information about some of the analysis and assumptions.

*Beam transport complexity:* the rows for ‘variable angles’ and ‘optical switch needed’ were added at the end of the scoring process to accommodate expected design perturbations, and are currently given zero weight. ‘Variable angles’ applies when an architecture requires a change in shape of the array, e.g. being able to change the aspect ratio of the X-Array. Any increased performance will be offset by an increase in the articulation range of the optics. An optical switch will be needed to switch between the two phasings of the Linear DCB described in Section 2.

*Control system complexity:* the number of control loops is estimated by

$$(\# \text{ metrology gauges}) + (\# \text{ fringe trackers}) + (\# \text{ angle trackers}) + (\# \text{ shear control points}),$$

where  $(\# \text{ metrology gauges}) = (\# \text{ collectors}) - 1 + (\# \text{ output beams}),$

$$(\# \text{ fringe trackers}) = (\# \text{ collectors}) - 1,$$

$$(\# \text{ angle trackers}) = (\# \text{ collectors}),$$

$$(\# \text{ shear control points}) = (\# \text{ collectors}) \times (\# \text{ beam hops to combiner}).$$

*Beam combiner optics complexity:* all four DCB architectures share the same 4-way beam combiner design. A different 3-way combiner is needed for the Triangle and Linear 3. Two different implementations were considered in each case: (1) a traditional co-axial combiner in which the beams are overlapped prior to coupling into a single-mode filter, and (2) a co-axial combiner in which spatially separated beams are coupled directly to the single-mode filter<sup>14</sup>. In both cases, the 4-way combiner was considered to be less complex than the 3-way combiner. The DCB beam combiner also only requires achromatic phase shifts of 0 and  $\pi$  radians, which opens up more implementation options.

*Number of mechanisms/moving parts:* the metric is  $\{(\# \text{ spacecraft}) \times (5 \text{ sunshade mechanisms}) + (\# \text{ collectors}) \times (1 \text{ secondary mirror deployment} + 1 \text{ thermal baffle} + 3 \text{ other}) + 1 \text{ cryocooler} + 1 \text{ high gain antenna}\}.$

*Difficulty of thermal control system:* the proximity factor accounts for the heating of a spacecraft by its near neighbors; the metric is proportional to the sum of the inverse square separations to the other spacecraft for the worst case spacecraft when observing a standard target. A low value means well-separated spacecraft with reduced thermal interactions.

*Fuel usage:* for a fixed rotation time, the total propulsive impulse needed to rotate the array is proportional to the sum of the products of mass and radius from the center of rotation for each spacecraft. The low weighting (1.7%) reflects the outcome of calculations indicating that the mass of fuel needed for the mission is not a major design driver.

*Adaptability to pre-launch predictions of Earth prevalence:* the star count calculations for determining the number of planets that can be characterized spectroscopically were predicated on an assumption that 10% of stars have terrestrial planets in the Habitable Zone. There is currently a large uncertainty in this value. A number of missions currently scheduled for launch prior to TPF-I, such as Kepler, COROT, SIM-PlanetQuest, and TPF-C, should help to refine our estimate considerably. A substantially smaller value would force us to look to more distant stars, for which smaller inner working angle and higher angular resolution will be at a premium. The sensitivity factor metric is given by the product of the modulation efficiency<sup>10,13</sup> and the total collecting area for the array.

*Concept maturity:* the scores here reflect the experience of NASA and its contractors with the features of the different architectures, and does not account for unpublished design work carried out by ESA and their contractors.

Table 5: Cost and risk discriminators, part 1

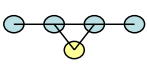
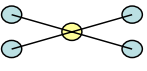
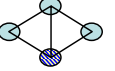
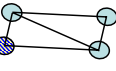
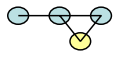
	Metric	Notes			Linear DCB		X-Array (2:1)		Diamond DCB		Z-Array		Triangle		Linear 3	
<b>Cost and Risk</b>																
Number of types of spacecraft	# types	Non-recurring design cost. Count mirror images as the same type. Excludes collector primary diameter (covered below)	4.7	1	7.0	3	10.0	2	7.0	3	5.0	4	7.0	3	7.0	3
Number of spacecraft	# spacecraft	Recurring cost (exclude complexity issues covered below)	2.6	1	6.5	5	6.5	5	8.0	4	8.0	4	10.0	3	8.0	4
Number of launches	# launches	Rendezvous. Extra launch cost. Increased risk of launch failure.	8.7	1	10.0	1	10.0	1	10.0	1	10.0	1	10.0	1	10.0	1
Mass margin	Mass margin	Greater design flexibility - above 30%	2.6	1	3.0	30%	<b>3.0</b>	30%	4.1	33%	4.1	33%	8.6	46%	5.5	37%
Equal size collector primaries	# distinct primary diameters	Non-recurring design cost for different telescope sizes	2.7	1	10.0	y	10.0	y	10.0	y	10.0	y	10.0	y	10.0	y
Beam transport optics complexity		Optical design. Excludes control loops.	4.1	1	7.0		10.0		7.0		4.5		7.0		7.0	
	# hops to combiner			1	7.0	2 hops	10.0	1 hop	7.0	2 hops	4.5	4 hops	7.0	2 hops	7.0	2 hops
	Variable angles			0	10.0	n	10.0	n	10.0	n	10.0	n	10.0	n	10.0	n
	Optical switch needed?			0		y	10.0	n	10.0	n	10.0	n	10.0	n	10.0	n
Control system complexity	# control loops	Includes metrology, fringe tracking, pointing loops. Excludes formation flying	4.8	1	8.3	22	<b>10.0</b>	18	8.3	22	<b>6.5</b>	26	9.6	19	9.6	19
Beamcombiner optics complexity		Optical design. Excludes control loops, metrology.	4.1	1	10.0	4-way	10.0	4-way	10.0	4-way	10.0	4-way	6.5	3-way	6.5	3-way
	Can it use 0 and 180 deg phases for nulling?			0.5	10.0	y	10.0	y	10.0	y	10.0	y	8.0	n	8.0	n
	# parts (from schematic)			0.5	10.0		10.0		10.0		10.0		5.0		5.0	
Number of mechanisms/moving parts	# mechanisms / deployments	Mechanisms can drive cost and robustness. Exclude optical mechanisms covered above. Include deployments, cryo-cooler	3.7	1	7.0	47	7.0	47	8.0	42	8.0	42	10.0	32	8.0	42
Difficulty of thermal control system		Major issue is # heat sources on the cold side of the spacecraft; also proximity of other spacecraft	2.6	1	5.9		8.4		5.3		4.4		7.3		7.5	
	# active sensors/mechanisms on cold side (worst collector)			0.375	6.3	9	<b>10.0</b>	5	6.3	9	<b>2.5</b>	13	6.3	9	6.3	9
	# active sensors/mechanisms on cold side (combiner)			0.375	6.3	36	6.3	36	4.2	41	<b>2.5</b>	45	7.9	32	<b>10.0</b>	27
	proximity factor			0.25	<b>5.0</b>	3.25	9.0	1.61	5.6	3	<b>10.0</b>	1.22	8.1	2	5.6	3



## 7. RESULTS AND DISCUSSION

The overall weighted scores for each architecture are given in Table 7. The X-Array has the highest score, followed by the Linear DCB. The Triangle and Linear 3 architectures failed one of the mandatory criteria (number of planets characterized by spectroscopy). It is worth emphasizing again that the weights and scores were iterated until they reflected the collective judgment of the group. The process is subjective, and a different group would be unlikely to arrive at exactly the same scores. While there were dissenting opinions on several of the discriminators, none were at a level to significantly change the overall outcome, and there was broad consensus on the final rankings.

Table 7: Weighted scores for single-launch options

	Linear DCB	X-Array (2:1)	Diamond DCB	Z-Array	Triangle	Linear 3
						
Overall score / 1000	<b>805</b>	<b>841</b>	<b>774</b>	<b>689</b>	<b>731</b> Failed	<b>772</b> Failed
Performance	370	365	323	280	244	319
Cost / risk	435	475	452	408	487	452

Even though the spread in scores between the top four options is less than 10%, the differences are significant. For example, one way for the Linear DCB to make up 36 points on the X-Array would be to introduce a new discriminator with a weighting of 5 and a difference in scores of 8. Because of the many contributors to the overall score, changing a single existing discriminator does not produce a large perturbation in the outcome. Table 8 shows a breakdown of the key discriminators – those that produce a swing of more than 10 points in the overall weighted scores – ranked by importance. The values shown give the swing in the weighted score, normalized relative to the Linear DCB option. It can be seen that the Triangle and Linear 3 gain in the cost and risk category, but not by enough to offset the penalty they incur in performance and graceful degradation.

Some of the metrics are common to multiple discriminators, giving the appearance of double book-keeping in the scoring. The philosophy adopted for the trade study was that this is actually a good feature – a metric that appears in multiple discriminators is shown to be an important design parameter. The number of spacecraft, for example, appears explicitly as a metric four times. The weights are applied to the discriminators, which should be addressing independent concerns and issues, not the metrics.

Discriminators can be re-weighted as technology development retires concerns, or as new problems become apparent. The addition of a new architecture requires that a new value is determined for each of the metrics, although in many cases the six existing architectures may already provide the values needed. The architectures studied have the bare minimum of functionality necessary for planet-finding, and the tables can be used to pinpoint specific design upgrades that will have the most benefit to a given architecture. Examples are the addition of optics for added redundancy, the capability to tune the aspect ratio of the X-Array and the addition of instrumentation to enhance the General Astrophysics performance.

One extension that was evaluated was the use of two Delta IV-Heavy launch vehicles for the Linear DCB and X-Array architectures. These two options had final scores of 789 (Linear DCB) and 823 (X-Array), slightly less than the corresponding scores for the single launch. The gain in performance in going from 3.8 m to 4.1 m aperture diameter and the additional mass margin was not considered enough to offset the cost and complexity of supporting two launches with a deep-space rendezvous. The number of launches required was easily the most highly weighted of the discriminators (Table 5). The two dual launch architectures are included in the last two columns in Table 8.

Table 8: Summary of key discriminators

<b>Discriminator</b>	<b>Metric</b>	Linear DCB	X-Array (2:1)	Diamond DCB	Z-Array	Triangle	Linear 3	Linear DCB (2 Launch)	X-Array (2 Launch)
Number of stars surveyed (beyond minimum required)	Star count	0	-9	-2	-43	-42	-5	3	-4
Number of launches	# launches	0	0	0	0	0	0	-44	-44
Number of planet systems characterized by spectroscopy at high angular resolution, beyond minimum required	Star count	0	2	-12	-11	-23	-23	5	4
Number of types of spacecraft	# types	0	14	0	-9	0	0	0	14
Beam transport optics complexity	# hops to combiner	0	12	0	-10	0	0	0	12
Redundancy / graceful degradation	Expected % of stars observed after loss of 1 spacecraft	0	4	-17	-6	-17	-17	0	4
Mass margin	Mass margin	0	0	3	3	15	6	18	18
Number of planet systems characterized by spectroscopy at low angular resolution, beyond minimum required	Star count	0	-8	-4	-14	-12	-7	4	-5
Difficulty of integration and test	# spacecraft	0	0	7	7	17	7	0	0
Control system complexity	# control loops	0	7	0	-7	5	5	0	7
Fidelity of image reconstruction	rms/peak (in Point Spread Function for planet at high res inner working angle)	0	-2	-6	-8	-14	-4	0	-2
Number of mechanisms/ moving parts	# mechanisms / deployments	0	0	4	4	11	4	0	0
General astrophysics potential	Dynamic range of baselines (max/min)	0	-4	-5	-10	-8	-4	0	-4
Complexity of flight operations	# spacecraft	0	0	4	4	10	4	0	0
Beamcombiner optics complexity	# parts (from schematic)	0	0	0	0	-10	-10	0	0

## 8. SUMMARY

A trade study was conducted to recommend an architecture for study by the TPF-I design team. Six architectures were considered: the Linear DCB, X-Array, Diamond DCB, Z-Array, Triangle and Linear 3. The telescope aperture size for each architecture was determined from the constraints of the Delta IV-Heavy launch vehicle using a parametric model. The architectures were first evaluated against a set of mandatory pass/fail criteria. The Triangle and Linear 3 arrays failed the criterion requiring more than 5 planets to be characterized by spectroscopy. The architectures were then scored against 27 different criteria, each of which had been assigned a weight, covering both performance and cost/risk issues. In the final weighted scores, the X-Array was rated the highest, followed by the Linear DCB, Diamond DCB, Linear 3, Triangle and Z-Array. We therefore recommend the X-Array for further study. The scoring process is inherently subjective. The tables presented in this paper should not be seen as a decision-making automaton; rather, they are intended to give clear insight into the engineering and scientific judgments that have been made.

This recommendation is not intended to preclude the consideration of new architectures; indeed, we hope that the work presented here will stimulate the development of new concepts and variants that can then be readily assessed against the existing architectures using the framework developed here.

## ACKNOWLEDGMENTS

The work described in this paper was performed at the Jet Propulsion Laboratory, California Institute of Technology, under contract with the National Aeronautics and Space Administration. M. C. Noecker was supported by JPL through contract #28000. J. A. Wertz receives support from the Michelson Fellowship Program through the Michelson Science Center. The authors are grateful for the contributions of many others at JPL, Ball, Lockheed Martin, Northrop Grumman, MIT, and elsewhere who have contributed to the understanding that is captured in this architecture recommendation.

## REFERENCES

1. N. Woolf and J. R. Angel, "Astronomical searches for earth-like planets and signs of life," *Ann. Rev. Astron. Astrophys* **36**, 507-537 (1998).
2. G. W. Marcy and R. P. Butler, "Detection of extrasolar giant planets," *Ann. Rev. Astron. Astrophys* **36**, 57-97 (1998).
3. R. N. Bracewell, "Detecting nonsolar planets by spinning infrared interferometer," *Nature* **274**, 780-781, (1978).
4. E. Serabyn, "Nulling interferometry and planet detection," in *Principles of long baseline interferometry*, P. Lawson, ed, (Jet Propulsion Laboratory, 2000), pp. 273-292.
5. D. Coulter, "NASA's Terrestrial Planet Finder mission: the search for habitable planets," in *Towards Other Earths: DARWIN/TPF and the search for extrasolar planets*, M. Fridlund and T. Henning, eds., (ESA Publications Division, Noordwijk, Netherlands, 2003), pp. 47-54.
6. A. Karlsson and L. Kaltenegger, "The technology of DARWIN," in *Towards Other Earths: DARWIN/TPF and the search for extrasolar planets*, M. Fridlund and T. Henning, eds., (ESA Publications Division, Noordwijk, Netherlands, 2003), pp. 41-46.
7. C. A. Beichman, N. J. Woolf, and C. A. Lindensmith, *Terrestrial Planet Finder: a NASA Origins program to search for habitable planets*, (Jet Propulsion Laboratory, 1999).
8. O. P. Lay, and S. Dubovitsky, "Nulling interferometers: the importance of systematic errors and the X-array," *Proc. SPIE* **5491**, 874-885, (2004)
9. A. L. Karlsson, O. Wallner, J. M. Perdigues Armengol, and O. Absil, "Three telescope nuller based on multibeam injection into single-mode waveguide," *Proc. SPIE* **5491**, 831-841, (2004)
10. S. Dubovitsky, and O. P. Lay, "Architecture selection and optimization for planet-finding interferometers," *Proc. SPIE* **5491**, 284-295, (2004)
11. M. C. Noecker, Z. Wei, and J. Decino, "Stray light estimates for the TPF formation flying interferometer," *Proc. SPIE* **5526**, 249-256, (2004)
12. Kepner, C. H. and Tregoe, B. B. *The New Rational Manager*. Princeton, NJ: Princeton Research Press (1981)
13. O. P. Lay, "Imaging properties of rotating nulling interferometers," *Appl. Opt.*, in press (2005)
14. O. Wallner, J. M. Perdigues Armengol, and A. L. Karlsson, "Multiaxial single-mode beam combiner," *Proc. SPIE* **5491**, 798-805, (2004)